Journal of Pharmaceutical Analysis 15 (2025) 101066

Contents lists available at ScienceDirect

Journal of Pharmaceutical Analysis

journal homepage: www.elsevier.com/locate/jpa

Original article

A tailored database combining reference compound-derived metabolite, metabolism platform and chemical characteristic of Chinese herb followed by activity screening: Application to Magnoliae Officinalis Cortex

Zhenzhen Xue [a, b], Yudong Shang [c], Lan Yang [b], Tao Li [d], Bin Yang [a, *]

[a] State Key Laboratory for Quality Ensurance and Sustainable Use of Dao-di Herbs, Institute of Chinese Materia Medica, China Academy of Chinese Medical Sciences, Beijing, 100700, China
[b] Artemisinin Research Center, China Academy of Chinese Medical Sciences, Beijing, 100700, China
[c] Institute of Antler Science and Product Technology, Changchun Sci-Tech University, Changchun, 130022, China
[d] Experimental Research Center, China Academy of Chinese Medical Sciences, Beijing, 10070, China

ARTICLE INFO

Article history:
Received 17 April 2024
Received in revised form
22 July 2024
Accepted 3 August 2024
Available online 8 August 2024

Keywords:
Tailored database
Metabolite traceability
Activity screening
Magnoliae Officinalis Cortex
In vivo metabolite

ABSTRACT

A strategy combining a tailored database and high-throughput activity screening that discover bioactive metabolites derived from Magnoliae Officinalis Cortex (MOC) was developed and implemented to rapidly profile and discover bioactive metabolites *in vivo* derived from traditional Chinese medicine (TCM). The strategy possessed four characteristics: 1) The tailored database consisted of metabolites derived from big data-originated reference compound, metabolites predicted *in silico*, and MOC chemical profile-based pseudomolecular ions. 2) When profiling MOC-derived metabolites *in vivo*, attentions were paid not only to prototypes of MOC compounds and metabolites directly derived from MOC compounds, as reported by most papers, but also to isomerized metabolites and the degradation products of MOC compounds as well as their derived metabolites. 3) Metabolite traceability was performed, especially to distinguish isomeric prototypes-derived metabolites, prototypes of MOC compounds as well as phase I metabolites derived from other MOC compounds. 4) Molecular docking was utilized for high-throughput activity screening and molecular dynamic simulation as well as zebrafish model were used for verification. Using this strategy, 134 metabolites were swiftly characterized after the oral administration of MOC to rats, and several metabolites were reported for the first time. Furthermore, 17 potential active metabolites were discovered by targeting the motilin, dopamine D2, and the serotonin type 4 (5-HT_4) receptors, and part bioactivities were verified using molecular dynamic simulation and a zebrafish constipation model. This study extends the application of mass spectrometry (MS) to rapidly profile TCM-derived metabolites *in vivo*, which will help pharmacologists rapidly discover potent metabolites from a complex matrix.

1. Introduction

Metabolites *in vivo* derived from traditional Chinese medicines (TCMs) are of great importance for elucidating the mechanisms of TCM, TCM quality control, and new drug discovery [1]. However, rapidly capturing the metabolic diversity of a TCM *in vivo* with high confidence remains a big challenge [2]. This is partly because of the complexity of TCM compounds and their metabolic pathways, which induce numerous TCM-derived metabolites and hinder their rapid detection. Similarly, the discovery of bioactive compounds from numerous metabolites is urgently needed.

Liquid chromatography-high-resolution mass spectrometry (LC-HRMS) is a powerful tool for metabolite characterization in TCM [3]. Owing to the poor understanding of the metabolic pathways of complex TCM constituents, most metabolism *in vivo* studies have focused on single compound [4–6]. To display the complex characteristics of TCM, strategies, such as from representative standards to single medicine and finally to prescription [7], representative compounds-metabolism platform-diagnostic extraction [8], and cross-mapping strategy from representative standards to herbal extracts and from high dose to clinical dose for herb-derived trace

* Corresponding author.
E-mail address: byang@icmm.ac.cn (B. Yang).

https://doi.org/10.1016/j.jpha.2024.101066

metabolite exploration, [9] have been proposed, in which extensive reference compounds were relied upon to first determine the metabolic pathways, hampering the application of these strategies. Targeted extraction using a database has recently become a key aspect of rapid metabolite detection in the post-processing of LC-HRMS data. Existing tools for metabolite prediction, e.g., as BioTransformer, the Chemical Transformation Simulator, and Systematic Generation of Potential Metabolites, can utilize reaction rules and machine learning methods to predict the phase I and II metabolism of small molecules [10]. However, these tools tend to overpredict even tens of thousands of predicted metabolites [11] and extra tools are needed to overcome the high rates of false positives and negatives. In addition, traceability analysis of TCM-derived metabolites is needed to increase confidence in structural identification and to elucidate their network relationships.

Magnoliae Officinalis Cortex (MOC), the stem bark of *Magnolia officinalis*, occurred in over 200 types of TCM formulae, has been used to treat abdominal distention and pain and dyspepsia for a long history [12]. To date, more than 200 compounds have been isolated from MOC, including lignans, phenylethanoid glycosides, phenolic glycosides, and alkaloid [13]. Studies on metabolites of MOC *in vivo* have mainly focused on two hydrophobic bioactive compounds [14,15]. Our group has isolated 24 novel phenylethanoid glycosides and phenolic glycosides from MOC water decoction, which is a traditional application form of TCM [12], and many of them showed potent cytotoxic activities, α-glucosidase inhibitory effects, and anti-functional dyspepsia activities [12,16]. Furthermore, we developed an LC-HRMS method for profiling and isomer recognition of phenylethanoid glycosides [17]. Notably, magnoloside A, a representative phenylethanoid glycoside, has prominent bioactivity, however, poor bioavailability [18], which indicated its metabolites *in vivo* are also bioactive components. Although other studies have attempted to detect *in vivo* metabolites after the oral administration of MOC extracts [19,20], only a few metabolites were detected. To the best of our knowledge, no report has provided the complete metabolic profile of the MOC water decoction.

In this study, we developed a strategy based on tailored database extraction and metabolite traceability analysis to rapidly profile metabolites with high confidence. The identified metabolites were then evaluated by high-throughput bioactivity screening, from which the bioactive ones were found. This strategy was named as TDAS (a tailored database combining reference compound-derived metabolites, metabolism platform, and TCM chemical characteristics followed by high-throughput activity screening) and is depicted in Fig. 1, and the discovery of bioactive metabolites of MOC in rats was used as an example.

2. Materials and methods

2.1. MOC materials, reference compounds, and MOC water decoction preparation

MOC samples authenticated as the stem bark of *Magnolia officinalis* were collected from Enshi, China and deposited at the Institute of Chinese Materia Medica, China Academy of Chinese Medical Sciences (Beijing, China). The reference compounds, magnolosides A, B, D, E, M, L, H, G, F, T, and S, and syringin, were isolated from the stem bark of *Magnolia officinalis* by our group. The other standard compounds used were commercial products. This structure is illustrated in Fig. S1. An MOC water decoction was prepared for oral administration to rats and profiled using LC-HRMS. The details are described in the Supplementary data.

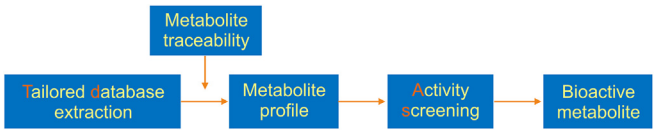

Fig. 1. Workflow of the tailored database followed by high-throughput activity screening (TDAS) strategy.

2.2. Animal experiments, bio-sample collection, and preparation

Male Sprague-Dawley rats (200 ± 20 g) were obtained from the Laboratory Animal Center of Peking University Health Science Center under license SCXK (Beijing) 2021-0013. All animal studies were reviewed and approved by the Institutional Animal Care and Use Committee of the Experimental Research Center, China Academy of Chinese Medical Sciences (Beijing, China) (Approval No.: ERCCACMS21-2111-01). The details of animal feeding and drug administration are described in Supplementary data.

Blood was collected from the angular vein at 0, 0.25, 0.58, 1, 2, and 6 h and centrifuged at 4,000 rpm for 15 min. Plasma samples were treated with three volumes of methanol to precipitate the proteins. After centrifuging at 10,000 rpm for 15 min, the supernatant was dried in vacuum at 40 °C, dissolved in 200 μL of methanol, and then filtered through a 0.22-μm membrane. The filtrates were mixed for LC-HRMS analysis. The rats were housed in metabolic cages (300 mm × 300 mm × 480 mm; Tecniplast China Co., Ltd., Shanghai, China), and urine and fecal samples were collected for 48 h. An aliquot of 5 mL of urine was loaded on a pretreated solid phase extraction (SPE) column (Oasis® HLB 6 cc (500 mg) LP Extraction Cartridge; Waters Corporation, Milford, MA, USA), washed with 5 mL of water, and then successively eluted with 5 mL of 5% methanol and 5 mL of methanol. The methanol eluate was collected and dried under vacuum at 37 °C. The residue was dissolved in 200 μL of methanol and filtered through a 0.22-μm membrane for LC-HRMS analysis. The feces were freeze-dried and ground into a crude powder. The powder (0.25 g) was subjected to extraction using 10 mL of methanol in an ultrasonic bath for 30 min. The resulting solution was dried and the residue was dissolved in 200 μL of methanol and filtered through a 0.22-μm membrane for LC-HRMS analysis.

2.3. LC-HRMS data acquisition and data process

An ACQUITY ultra-performance liquid chromatography (UPLC)™ system coupled with a SYNAPT™ XS mass spectrometer (Waters Micromass, Manchester, UK) was used to obtain data-independent acquisition (DIA) data, i.e., MS^E. A Waters ACQUITY UPLC HSS T_3 column (2.1 mm × 100 mm, 1.8 μm) coupled with a Waters Van Guard T3 pre-column (2.1 mm × 5 mm, 1.8 μm) was adopted and a temperature of 40 °C was applied. The mobile phases were 0.1% (*V*/*V*) formic acid aqueous solution (A) and 0.1% (*V*/*V*) formic acid acetonitrile (B) with the following gradient: 5%–20% B (0–12 min), 20%–40% B (12–13 min), 40%–60% B (13–15 min), 60%–70% B (15–18 min), and 70%–90% B (18–23 min). The equilibration time and flow rate were set to 4 min and 0.4 mL/min, respectively. The sample injection volume was 1 μL. The temperature of the autosampler chamber was set at 4 °C. The MS parameters in negative mode were set as follows: mass range, 50–1200 Da; analyzer mode, resolution; dynamic range, normal; scan time, 0.2 s; data format, continuum; ramp trap collision energy, 35–60 V; capillary, −2.0 kV; source temperature, 100 °C; sampling cone, 40 V; desolvation temperature, 450 °C; cone gas flow, 50 L/h; and desolvation gas flow, 900 L/h. In the positive mode, the parameters were identical to those in the negative mode, except for the ramp trap collision energy (25–30 V) and capillary voltage (+0.5 kV). Data acquisition was controlled using MassLynx

V4.1 software (Waters Corporation). To obtain data-dependent acquisition (DDA) data, a Vanquish ultra-high performance liquid chromatography (UHPLC) system coupled with an Orbitrap Exploris 240 mass spectrometer (Thermo Fisher Scientific Inc., Waltham, MA, USA) was used, as described in the Supplementary data.

Unified science informatics platform (UNIFI) 1.8 (Waters Corporation) was used for the prediction and characterization of metabolites. Key parameters within UNIFI were set as follows: 1) peak rejection, minimum area of 500.0; 2) manually specified retention time range, 0.5–26.0 min; 3) intensity threshold, 300.0 counts for low energy acquisition and 40.0 counts for high energy acquisition; 4) target match tolerance and fragment match tolerance, 10.0 mDa; 5) selected negative adducts, $HCOO^-$, −H; 6) selected positive adducts, +H, −e; 7) maximum number of transformation, two for phase I and one for phase II; 8) mass error for component identification is less than or equal to 5 mDa and 5 ppm; and 9) response for component identification is greater than 10,000 for the alkaloid-derived metabolites, >1,000 for the lignan-derived metabolites, and >5,000 for the degradation product-derived metabolites.

2.4. Strategy and methodology

The present study aimed to rapidly profile MOC-derived metabolites *in vivo* and efficiently discover potent metabolites. As shown in Fig. 1, the proposed TDAS strategy stands out in the following four aspects:

2.4.1. Tailored database construction

The database includes metabolites derived from big data-originated reference compounds, metabolites predicted *in silico*, and MOC chemical profile-based pseudomolecular ions. The metabolites derived from the reference compounds were collected by retrieving literature from Web of Science and PubMed using the keywords “metabolism”, “phase I”, “phase II”, and the name of the reference compounds. It should be mentioned that the collected reference compounds not only included MOC chemicals but also included their isomers and degradation products, such as aglycones and aromatic acids, because previous studies have found that TCM compounds are usually degraded by intestinal bacteria [21]. Similarly, the metabolites predicted *in silico* also contained those derived from compounds in the MOC and their degradation products, in which UNIFI was employed by importing the targeted components, selected transformations, and optimized parameters.

2.4.2. Profiling MOC-derived metabolites in vivo

When profiling MOC-derived metabolites *in vivo*, attention was paid not only to prototypes of MOC compounds and metabolites directly derived from MOC compounds, as most papers have reported, but also to isomerized metabolites and the degradation products of MOC compounds as well as their derived metabolites. The prototypes of MOC compounds as well as their isomerized metabolites and degradation products of MOC compounds were characterized by extracting MOC chemical profile-based pseudomolecular ions. Metabolites directly derived from both MOC compounds and degradation products were characterized using *in silico* auto-characterization and matched with the big data-originated reference compound-derived metabolites. UNIFI can efficiently realize precursor and product ion auto-retrieval in the experimental mass spectra. The structures of the potential metabolites were further identified by manual analysis of their HRMS and MS/MS spectra.

2.4.3. Metabolite traceability analysis

Metabolite traceability was determined to distinguish the isomeric prototype-derived metabolites, prototypes of MOC compounds, and phase I metabolites derived from other MOC compounds. Representative reference compound-derived metabolic profiles were acquired from the animal experiments. Mixed metabolites derived from MOC were traced and compared with the targeted compound-derived metabolic profile and MOC water decoction chemical profile. In addition, DDA-aided MS^E analysis was used to increase the metabolite assignment confidence, which not only acquired better MS/MS spectral coverage, but also circumvented the misassignment of fragment ions to co-eluting precursor ions [22].

2.4.4. High-throughput activity screening

Molecular docking was performed by targeting the motilin receptor (Protein Data Bank (PDB) ID: 8IBU), dopamine D2 receptor (PDB ID: 7DFP), and the serotonin type 4 (5-HT_4) receptor (PDB ID: 7XT8) to identify MOC-derived metabolites with potential activities for promoting gastrointestinal motility. AutoDock 4.2 and AutoDockTools 1.5.6 were used for molecular docking [23]. Residue-ligand interactions were evaluated using a Protein-Ligand Interaction Profiler [24]. Molecular dynamic simulation and a zebrafish constipation model were used to verify the potency of the candidate metabolites. Molecular dynamic simulations were performed on a Dell Precision 7920 workstation using the AMBER20 software package [25], and the leaprc.protein.ff19sb force field was used for energy minimization and molecular dynamic simulations. The detailed methodologies are described in the Supplementary data.

3. Results and discussion

3.1. Tailoring the integrated database

A tailored database was constructed for metabolites derived from big data-originated reference compounds, metabolites predicted *in silico*, and MOC chemical profile-based pseudomolecular ions. By anatomizing the literature in the Web of Science and PubMed, 192 metabolites with their names, molecular weights, molecular formulas, and corresponding references were collected (Fig. S2). In addition to 170 metabolites derived from the MOC reference compounds, 22 metabolites from their isomers and degradation products were included. Meanwhile, 309 compounds isolated from MOC with information on generic name, molecular weight, molecular formula, and structural formula were determined by searching SciFinder^n Scholar. Based on literature data and our previous methods [17,26], a total of 122 compounds (55 phenylethanoid glycosides, 20 phenolic glycosides, 7 lignan glycosides, 19 lignans, 16 alkaloids and 5 other compounds) were identified in MOC water decoction chemical fingerprint (Fig. 2 and Table S1); details are described in Supplementary data. Moreover, 14 pseudomolecular ions (*m/z* 265, 281, 314, 342, 401, 417, 447, 461, 477, 609, 623.2187, 623.1976, 771, and 785), which covered the major types of MOC compounds, were selected based on their intensity from the full-scan mass spectra in the LC-HRMS analysis (Figs. S3 and S4). Eight types of aglycones and substituted aromatic acids (i.e., methoxytyrosol, 3,4,5-trimethoxyphenol, hydroxytyrosol, tyrosol, 3-hydroxyphenylethanol, caffeic acid, sinapyl alcohol, and ferulic acid) were acquired based on the MOC chemical profile analysis. Finally, 12 targeted components, including magnolol, honokiol, obovatol, piperitylmagnolol, (*R*)-magnocurarine, (*S*)-magnoflorine, 3,4,5-trimethoxyphenol, sinapyl alcohol, caffeic acid, ferulic acid, hydroxytyrosol, and tyrosol were imported into UNIFI to predict 207 metabolites using reported transformations (19 metabolic pathways for lignans, 7 for alkaloids, and 5 for degradation products) and optimized UNIFI parameters. Their HRMS and MS/MS spectra were further analyzed in the following section to

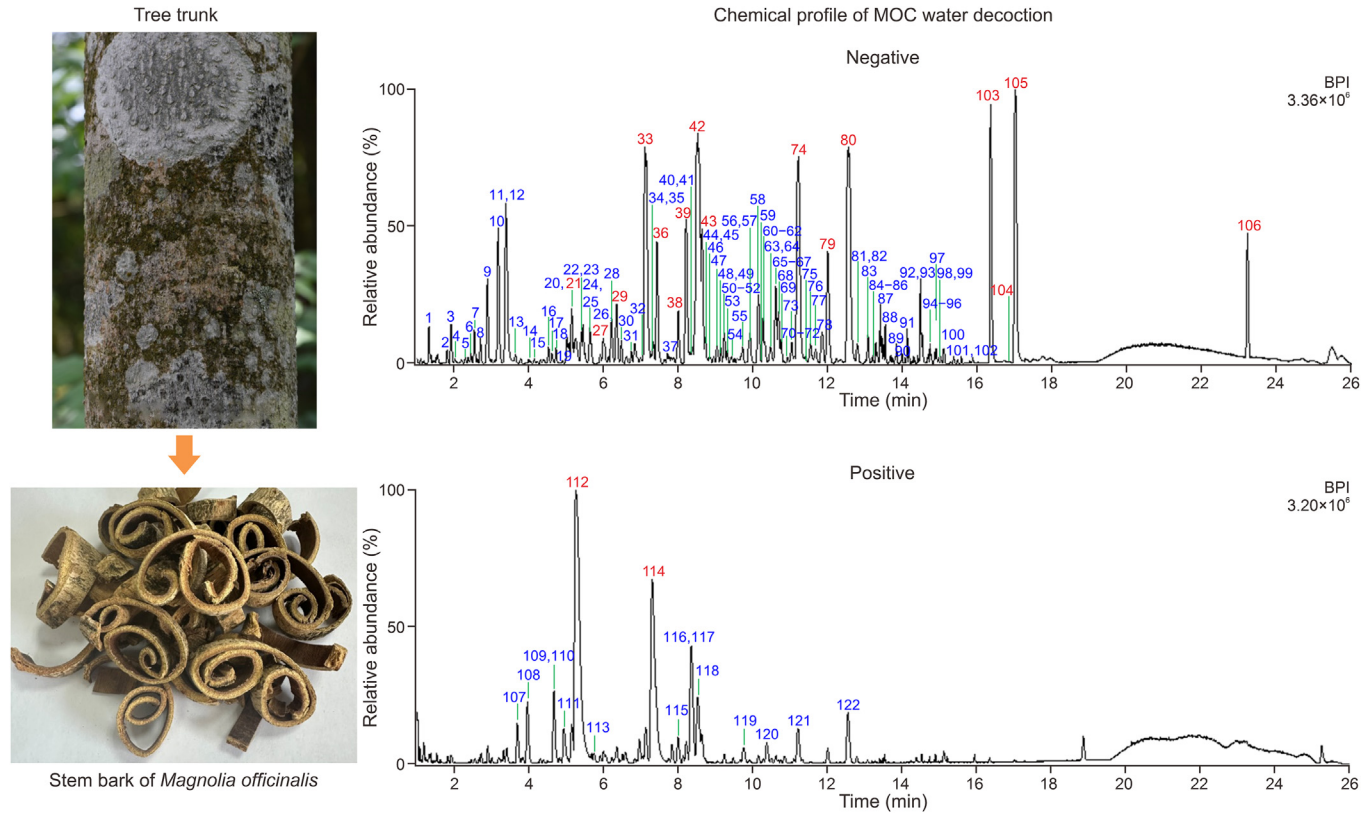

Fig. 2. Chemical profile of Magnoliae Officinalis Cortex (MOC) water decoction by ultra-performance liquid chromatography coupled with quadrupole time-of flight mass spectrometry (UPLC-QTOF/MS). Compounds confirmed by reference standards are marked in red. BPI: base peak ion chromatogram.

identify the structures. In conclusion, the tailored database contained information on MOC chemicals and their isomers and degradation products, including aglycones, small molecules of aromatic acids, and their derived metabolites. The database expanded the extraction coverage and contained the characteristics of the TCM itself.

3.2. Rapid profiling of MOC-derived metabolites in vivo using tailored database and metabolite traceability

Using the TDAS strategy, 134 metabolites were identified from the MOC-derived metabolic profile, including 41 prototypes and their isomerized metabolites, 60 metabolites directly derived from MOC compounds, and 33 degradation products and their derived metabolites. Among them, 49 metabolites were detected by the extraction of pseudomolecular ions, 35 were predicted and identified by UNIFI, and 50 were identified by matching metabolites derived from big data-originated reference compounds. In addition, the origins of the 38 metabolites were confirmed using reference compounds.

The prototypes of MOC compounds and their isomerized metabolites are mainly derived from phenylethanoid glycosides, phenolic glycosides, lignans, and alkaloids. Pseudomolecular ions in the tailored databases were used to extract prototypes *in vivo*, and their structures were confirmed by comparing the retention time, MS, and MS/MS data, with the results in Table S1. The extract ion chromatograms (EICs) of *m/z* 265.1229, 623.1976, and 785.2504 were analyzed in detail. After extracting the ion at *m/z* 265.1229, eight and two peaks were found in the plasma and feces, respectively, whereas no peaks were detected in the urine under current conditions (Fig. 3A). By comparing the retention time and MS data in Table S1, $M0_1$ and $M0_2$ were characterized as honokiol and magnolol, respectively. M1, M2, M4, and M5 were identified as honokiol isomers owing to the existence of characteristic fragment ions at *m/z* 249, 224, and 223, whereas M3 and M6 were characterized as magnolol isomers because of the typical fragment ions at *m/z* 247 and 245 (Fig. S5). The ratio of the peak area of honokiol to that of magnolol in the MOC water decoction, feces, and plasma decreased sequentially (Area$M0_1$/$M0_2$, 0.77, 0.46, and 0.02). Particularly in the plasma, as the level of honokiol decreased, the levels of its isomers M1, M2, M4, and M5 increased. Isomers M3 and M6 derived from magnolol were also detected. Magnolol isomers isomagnolol and 5-allyl-5'-(1-propen-1(*E*)-yl)-2,2′-dihydroxybiphenyl were reported to be detected in feces by repeated oral administration of magnolol to rats [27]. As isomagnolol has a weaker antibacterial action than magnolol, isomerization of magnolol is likely to be one of the detoxification processes by intestinal bacteria [27]. However, in the current study, the magnolol isomers M3 and M6, as well as honokiol isomers M1, M2, M4, and M5 were first found in plasma samples rather than in feces following a single administration of MOC water decoction to rats. Isomerized metabolites of honokiol and magnolol have the potential to be used as effective ingredients. The second example was obtained by the extraction of *m/z* 623.1976, which exhibited six and one peaks in feces and urine samples, respectively, whereas no peak was extracted in plasma (Fig. 3B). Peaks $M0_{23}$−$M0_{28}$ were all characterized as prototypes by comparing the retention times and MS data in Fig. S6 and Table S1. $M0_{23}$, $M0_{27}$, and $M0_{28}$ were unambiguously identified as magnolosides A, M, and D, respectively. The ratio for the peak area of magnoloside D to magnoloside A was declined sharply in feces (Area$M0_{28}$/$M0_{23}$, 0.02), which was 0.84 in MOC water decoction. Meanwhile, the ratio of the peak areas of $M0_{25}$ and $M0_{26}$, especially $M0_{25}$, to magnoloside A in feces (Area$M0_{25}$/$M0_{23}$, 0.54) was increased compared to that in the MOC water decoction (Area$M0_{25}$/$M0_{23}$, 0.10). Although magnoloside D was the most stable among the homologous compounds of

magnolosides A, M, and D [28], magnoloside D was more prone to isomerization or degradation by intestinal bacteria in the current study, indicating an intense interaction between magnoloside D and the gut microbiota. For filtering with *m/z* 785.2504, four and three prototypes were observed in the feces and urine samples, respectively (Fig. S7). $M0_{31}$ and $M0_{33}$ were identified as magnolosides B and F, respectively, by comparing their retention times and MS data (Table S1). In contrast to the detection of the diglycoside magnoloside A in urine, the triglycosides magnoloside B, F, and $M0_{34}$ were detected in urine samples. However, those were absent in the plasma sample, which was consistent with the diglycoside results.

In addition to *m/z* 265.1229, 623.1976, and 785.2504, the other 11 pseudomolecular ions ($[M-H]^-$, $[M+HCOO]^-$, $[M]^+$, *m/z* 281, 314, 342, 401, 417, 447, 461, 477, 609, 623.2187, and 771) were also used to extract exposed chemicals *in vivo* (Fig. S8). A total of 34, 14, and 14 compounds were detected in the fecal, plasma, and urine samples, respectively (Table S2). Among these, compounds $M0_1-M0_{34}$ were prototypes and compounds M1−M7 were prototype-derived metabolites by isomerization transformation. As the results suggested, the prototypes of phenylethanoid glycoside were mainly detected in feces and hardly detected in plasma, which were similar to those of alkaloids mainly detected in feces; phenolic glycoside prototypes could be detected in both plasma and urine, and the prototypes of lignans could be detected in plasma and feces, however, were hardly detected in urine.

The degradation products of MOC compounds as well as their derived metabolites were mainly derived from phenylethanoid glycosides and phenolic glycosides [6,29]. Orally administered glycosides are prone to hydrolysis by intestinal flora [30]. Eight degradation products, i.e., methoxytyrosol (M8), 3,4,5-trimethoxyphenol (M9), hydroxytyrosol (M14), tyrosol (M18), 3-hydroxyphenylethanol (M23), caffeic acid (M29), sinapyl alcohol (M36), and ferulic acid (M37), were detected in the feces. Among these, M14, M29, and M37 were unambiguously identified by comparison with reference compounds. Subsequently, the *in silico* metabolites were predicted by UNIFI through the metabolic reactions of reduction [6], dihydroxylation [6], glucuronidation, sulfation, and methylation [6] and the MS/MS product ions of the 12 predicted metabolites were further confirmed in DDA mode (Table S3). Among the identified metabolites, sulfate and glucuronide conjugates produced diagnostic fragments of $[M-H-80]^-$ and $[M-H-176]^-$ in the MS/MS spectra, respectively [19]. The characterization of metabolites derived from caffeic acid by the reduction reaction is shown in Fig. 4A, which produced a molecular ion of *m/z* 181.0498 and a fragment ion of *m/z* 135.0443. In addition, by searching the reference compound-derived metabolites in a tailored database, one acetylated phenylethanoid glycoside (M50), which produced a fragment ion of $[M-H-42]^-$, was detected in feces [6], and 12 degradation product-derived metabolites were detected in plasma and urine (Table S3), and their MS/MS data were compared to those reported in the literature [6,20]. In total, 19, 6, and 12 degradation products and their derived metabolites were putatively identified in plasma, urine, and feces, respectively. The degradation products and their reduced and methylated metabolites were mainly detected in feces, and extensive metabolites derived from the degradation products were detected in the plasma.

The metabolites directly derived from MOC compounds were mainly lignans and alkaloids (isomerized metabolites were not included). By searching a tailored database, 37 metabolites derived from lignans were detected in plasma, urine, and feces [18,31]. Database extraction-aided characterization of lignan-derived metabolites (molecular formula: $C_{24}H_{24}O_{13}S$) was performed in detail (Fig. 4B). After extracting the molecular ion at *m/z* 551.0859, seven high-intensity peaks were detected in the plasma sample. By analyzing their mass spectra at both low and high energies, four peaks, M40 (10.46 min), M43 (11.84 min), M45 (11.97 min), and M48 (12.64 min) with prominent molecular ions at *m/z* 551.0859 and product ions at *m/z* 295.0999 and 251.1073 were identified as honokiol-derived metabolites (Table S3). In addition, 19 alkaloid-derived metabolites and four lignan-derived metabolites were predicted and characterized using UNIFI (Table S3). Hydroxylation, demethylation, desaturation, acetylation, methylation, glucuronidation, and sulfation are the primary reactions for alkaloid [32]; whereas oxidation, methylation, acetylation, dehydrogenation, reduction, carboxylation, glucuronidation, sulfation, and amino acid conjugation are the major reactions for lignins [18,31].

Finally, the experimental data of some reference compound-derived metabolic profiles were obtained to confirm the origins of the MOC-derived metabolites. First, MOC-derived metabolites M51, M52, M61, M63−M67, M71−M74, M77, M78, M80, and M81 originated from magnolol, whereas metabolites M41, M42, M49, M53−M60, M69, M75, and M76 were identified based on honokiol. Representative chromatograms of the MOC/honokiol/magnolol-derived metabolites with a molecular ion at *m/z* 361.0750 are shown in Fig. S9A. In addition to the reported product ions of *m/z* 281 and 263 for M56 and M65 [18], an additional typical product ion of *m/z* 222.0682 from M56 and an ion of *m/z* 245.0950 from M65 were also observed in the current study and further confirmed in the DDA-MS/MS spectra (Fig. S9A), which could be further used to distinguish the metabolites derived from honokiol or magnolol. Second, MOC-derived metabolites M11, M13, and M14 were detected in both magnoloside A- and hydroxytyrosol-treated biosamples, and metabolites M24, M26, and M29 were detected in both magnoloside A- and caffeic acid-treated biosamples. The results indicated glycoside in TCM may act as prodrugs [30]. Third, MOC-derived metabolites M68 and M79 were traced as minor prototypes that could be detected in the MOC water decoction (93 and 102, respectively) and were not found to be phase I metabolites of honokiol and magnolol under the current conditions [15] (Fig. S9B). In addition, MOC-derived metabolites M64, M73, and M78 were found not only in the phase I oxidative metabolites of magnolol, but also in the minor prototypes that could also be detected in the MOC water decoction (91, 97, and 101, respectively) (Fig. 5). These results indicate that some of the major prototypes could be metabolized into other minor prototypes and have synergistic effects *in vivo*.

In conclusion, lignans are prone to direct transformation into metabolites mainly via oxidation, reduction, isomerization, glucuronidation, and sulfation. In contrast, phenylethanoid glycosides are prone to hydrolysis into degradation products, which can be further subjected to reduction, glucuronidation, sulfation, and methylation.

Compared to the conventional strategies [7−9], the established TDAS strategy herein possessed four characteristics. 1) It enlarged the volume of data in the database, in which metabolites derived from big data-originated reference compound, metabolites predicted *in silico*, and compounds in MOC were included. 2) More kinds of metabolites were accordingly discovered, i.e., besides prototypes of MOC compounds and metabolites directly derived from MOC compounds, which most papers reported, isomerized metabolites and the degradation products of MOC compounds as well as their derived metabolites were found using TDAS, e.g., the isomerized metabolites of magnolol and honokiol were firstly found in rat plasma sample, and the degradation product of ferulic acid as well as its reduced metabolite were found in feces sample and its sulfated metabolite was found in plasma. 3) The origins of some MOC-derived metabolites were traced to elucidate their network relationship, e.g., M64, M73, and M78 were not only found

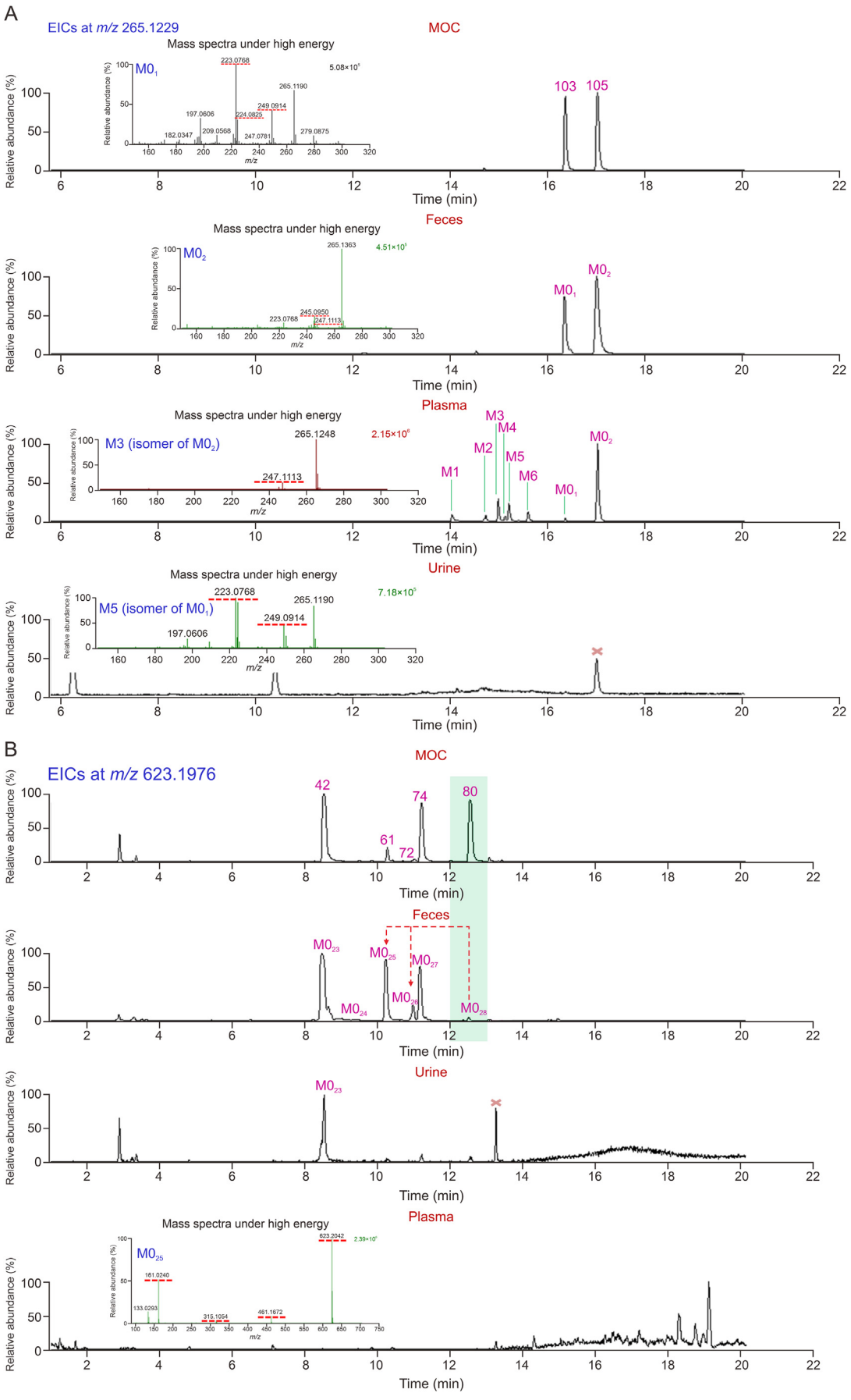
A
EICs at m/z 265.1229
MOC
Mass spectra under high energy
M0$_1$
223.0768
5.08×10^5
265.1190
249.0914
197.0606
224.0825
182.0347
209.0568
247.0781
279.0875
103
105
Relative abundance (%)
Time (min)
Feces
Mass spectra under high energy
M0$_2$
265.1363
4.51×10^5
245.0950
223.0768
247.1113
M0$_1$
M0$_2$
Plasma
Mass spectra under high energy
M3 (isomer of M0$_2$)
265.1248
2.15×10^6
247.1113
M1
M2
M3
M4
M5
M6
M0$_1$
M0$_2$
Urine
Mass spectra under high energy
M5 (isomer of M0$_1$)
223.0768
265.1190
7.18×10^5
249.0914
197.0606
B
EICs at m/z 623.1976
MOC
42
74
80
61
72
Feces
M0$_{23}$
M0$_{25}$
M0$_{27}$
M0$_{26}$
M0$_{24}$
M0$_{28}$
Urine
M0$_{23}$
Plasma
Mass spectra under high energy
M0$_{25}$
623.2042
2.39×10^7
161.0240
133.0293
315.1054
461.1672

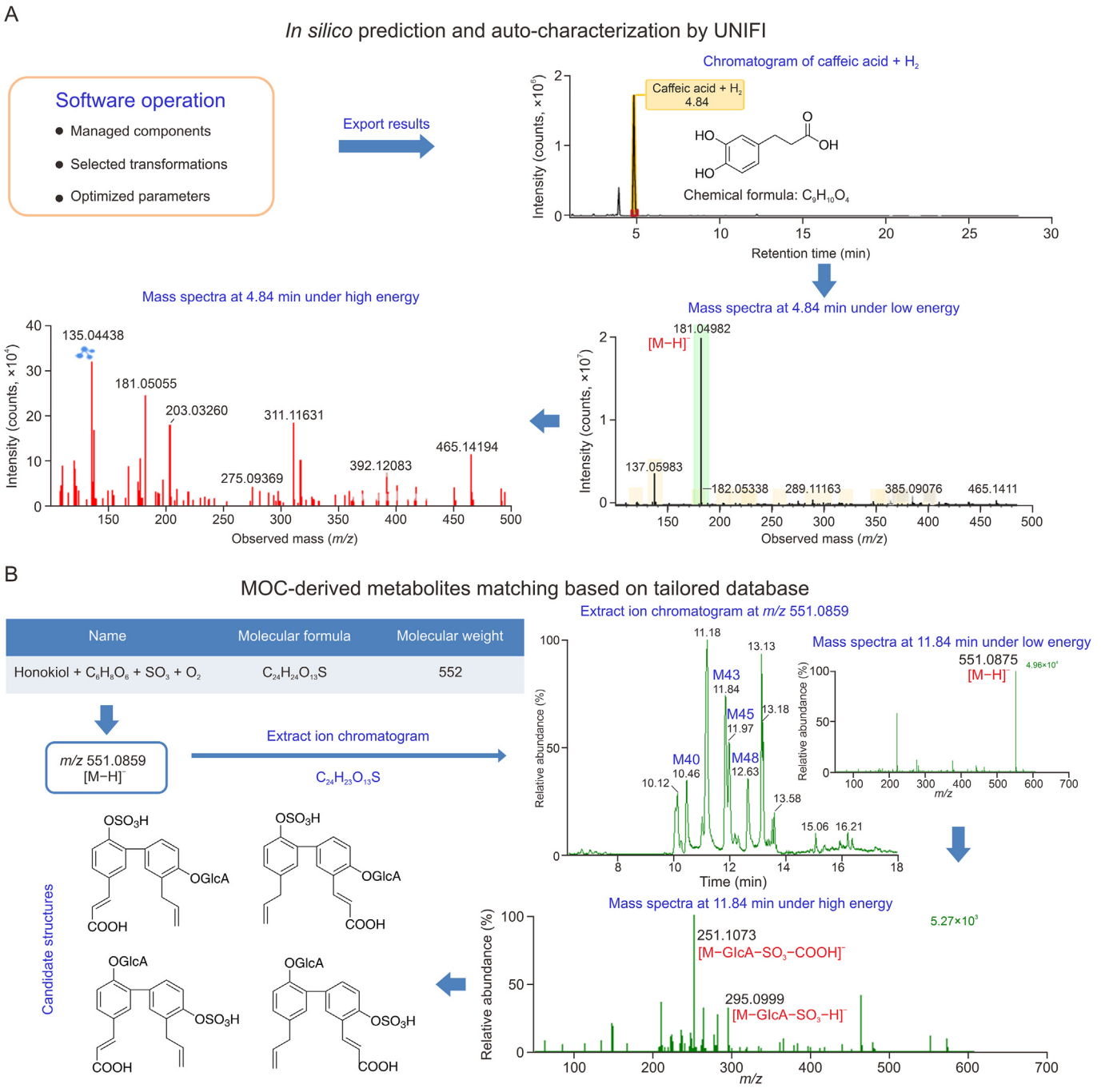

Fig. 4. Characterization of metabolites. (A) *In silico* prediction and auto-characterization by unified science informatics platform (UNIFI). (B) Magnoliae Officinalis Cortex (MOC)-derived metabolites matching using the tailored database. The inset indicates the mass spectra under low energy of the peak at 11.84 min.

as the major compound magnolol-derived metabolites, but also the prototypes of other minor lignans. 4) Molecular docking was utilized for high-throughput activity screening.

In addition, both DDA and DIA were employed to identify metabolite structures. Although the Orbitrap Exploris 240 mass spectrometer can perform both DDA and DIA experiments, the responses of some components in the MOC were extremely low when using the Orbitrap Exploris 240 mass spectrometer, whereas they were high when using the SYNAPTTM XS mass spectrometer. To detect more peaks with high responses and high-quality MS^2

Fig. 3. Metabolites detection by extracting pseudomolecular ions. (A) Extract ion chromatograms (EICs) at *m/z* 265.1229 (103/$M0_1$: honokiol; 105/$M0_2$: magnolol; M1/M2/M4/M5: honokiol isomers; and M3/M6: magnolol isomers). (B) EICs at *m/z* 623.1976 (42/$M0_{23}$: magnoloside A; 74/$M0_{27}$: magnoloside M; and 80/$M0_{28}$: magnoloside D). The insets indicate mass spectra under high energy of $M0_1$, $M0_2$, M3, M5, and $M0_{25}$, respectively. The red crosses indicate the peaks were not identified as $M0_2$ and $M0_{28}$, respectively. MOC: Magnoliae Officinalis Cortex.

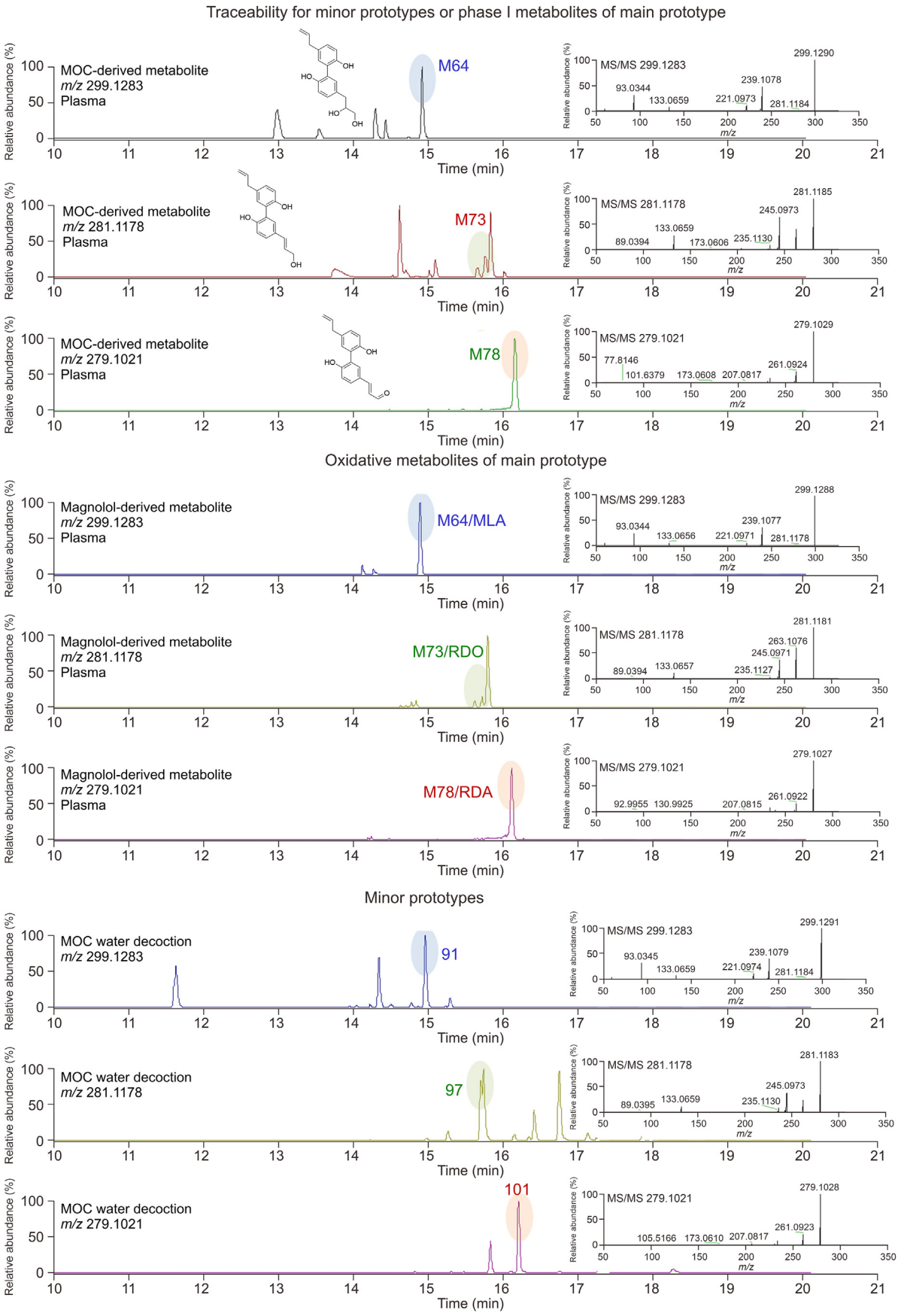

Fig. 5. Traceability analysis for Magnoliae Officinalis Cortex (MOC)-derived metabolites *in vivo*. Traceability for minor prototypes or phase I metabolites of main prototype. The insets indicate tandem mass spectrometry (MS/MS) spectra of M64, M73, M78, MLA, RDO, RDA, 91, 97, and 101, respectively. MLA: magnolignan A; RDO: randainol; RDA: randainal.

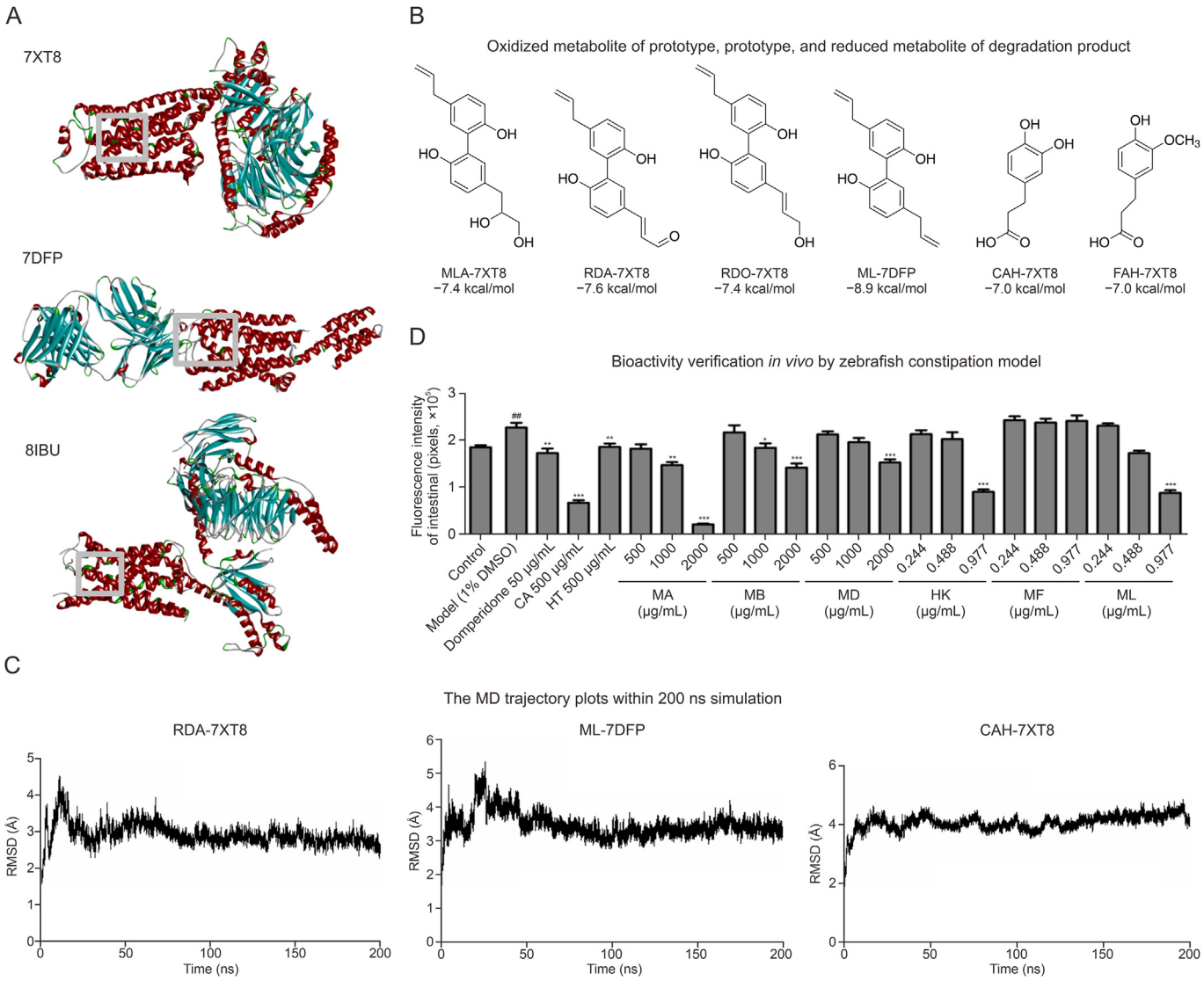

Fig. 6. Discovery of potent metabolites using high-throughput bioactivity screening. (A) Active pockets of serotonin type 4 (5-HT_4) receptor (Protein Data Bank (PDB) ID: 7XT8), dopamine D2 receptor (PDB ID: 7DFP), and motilin receptor (PDB ID: 8IBU). (B) Potential hit metabolites: magnolignan A (MLA) (M64); randainal (RDA) (M78); randainol (RDO) (M73); magnolol (ML) ($M0_2$); 7,8-dihydrocaffeic acid (CAH) (M24); and 7,8-dihydroferulic acid (FAH) (M35). (C) The molecular dynamic (MD) trajectory plots within 200 ns simulation for RDA-7XT8, ML-7DFP, and CAH-7XT8 complexes. (D) Bioactivity verification *in vivo* by zebrafish constipation model. $^{*}P < 0.05$, $^{**}P < 0.01$, and $^{***}P < 0.001$, compared to the model group (1% dimethyl sulfoxide (DMSO)); $^{\#\#}P < 0.01$, compared to the control group.

spectra, both instruments with their featured data acquisition modes were used in current study.

3.3. Potent metabolites discovery based on high-throughput activity screening

Traditionally, MOC have been used to treat abdominal distention and dyspepsia. Motilin, dopamine D2, and 5-HT_4 receptors were the most common targets for gastrointestinal prokinetic agents [33,34]. Given the occurrence of gastrointestinal motility disorders was ascribed to a combination of multiple factors and the action mode of TCM was "multi-targets", motilin receptor (PDB ID: 8IBU), dopamine D2 receptor (PDB ID: 7DFP) and 5-HT_4 receptor (PDB ID: 7XT8) were employed to screen the candidate metabolites. The interesting exposed prototypes, the first prototype-derived isomerized metabolites, representative MOC compound-derived metabolites, the parent compounds degraded in the gut or interacted intensely with the gut microbiota, and the degradation products and their derived metabolites (Fig. S10) were screened. The active pockets of the motilin receptor (PDB ID: 8IBU), dopamine D2 receptor (PDB ID: 7DFP), and 5-HT_4 receptor (PDB ID: 7XT8) are shown in Fig. 6A. The results obtained by targeting the motilin and dopamine D2 receptors indicated that the degradation products and their derived metabolites showed lower affinities than their parent compounds and other types of metabolites (Tables S4 and S5). For the 5-HT_4 receptor, the isomerized metabolites of honokiol and magnolol, honokiol, the oxidized metabolites of magnolol, and the reduced metabolites of caffeic acid and ferulic acid showed high affinities compared to the positive drug mosapride, whereas the parent compounds of magnolosides A, B, D, and M showed weaker affinities (Table S6). Totally, 17 representative metabolites were discovered as the potent metabolites (<−7.0 kcal/mol) (Figs. 6B and S11), in which three metabolites were oxidized metabolites of prototypes, two were reduced metabolites of degradation products, five were isomerized metabolites of prototypes, and the others were prototypes or MOC parent compounds. Motilin and

dopamine D2 receptors showed similar tendencies; thus, their molecular interactions with different types of components were further analyzed. Hydrophobic interactions, hydrogen bond interactions, salt bridge interactions, and π−π stacking were the major interactions between ligand and receptor (Figs. S12 and S13). The results indicated that common interaction sites were present among similar types of compounds and different common interaction sites were observed between different compounds and positive drugs (Tables S7 and S8). This explains the differential activity of the compounds compared with that of the positive control drug. In addition, the interaction results showed that the common interaction site of magnolosides A, B, and D with motilin receptor, i.e., Leu341 was also the active site of erythromycin with the motilin receptor [33]. Phe110, a common interaction site of magnolosides A, B, D, and domperidone with the dopamine D2 receptor (7DFP) [35], is also the active site of risperidone, domperidone, and naringenin on the dopamine D2 receptor (6CM4) [36]. The above results also confirm the validity of the molecular interactions in the current study. Furthermore, molecular dynamic simulations were performed to ensure the stability of the ligand-target interactions with respect to time. The root-mean-square deviation (RMSD) plots for three representative complexes were listed in Fig. 6C and the smooth molecular dynamic trajectories (the mean values of RMSD < 4 Å and the fluctuating values < 1 Å) indicated the ligand-target interactions were stable with respect to time. Meanwhile, the tendency of binding free energies between complexes of RDA-7XT8 (randainal-7XT8, −17.3 kcal/mol) and CAH-7XT8 (7,8-dihydrocaffeic acid-7XT8, −10.8 kcal/mol) in Table S9 was consistent to that of docking energies (Fig. 6B), which also indicated the validity of molecular docking screening.

Zebrafish have proven to be a great tool to model human diseases, not only because their embryos and larvae are virtually transparent during development, allowing visualization of internal organs in a noninvasive manner, but also because approximately 71.4% of human proteins have at least one zebrafish ortholog [37]. A previous study found that the gastrointestinal tract of zebrafish displays an anatomy and cellular architecture similar to that of humans [38], and the 5-HT system in zebrafish is similar to that of mammals [39]. Sequence alignments of dopamine D2 and 5-HT_4 receptors of zebrafish to those of humans were performed, from which 61.82% and 75.60% similarities were obtained, respectively. Accordingly, an aluminum sulfate-induced zebrafish constipation model was developed in current study to verify the *in vivo* efficacy of the candidate metabolites (Fig. S14). Details of the administered dosages are provided in Table S10. The fluorescence intensity of the zebrafish gut was measured and a typical map after sample treatment is shown in Fig. S15. The results in Fig. 6D demonstrated that the intestinal fluorescence intensity in model group (1% dimethyl sulfoxide (DMSO)) was significantly higher than that of control group ($P < 0.01$) and the positive drug of domperidone at 50 μg/mL could significantly decrease the intensity ($P < 0.01$), which indicated the constipation model was successfully established. Magnoloside A at a medium dose (1.60 mM), magnoloside D at a high dose (3.20 mM), and magnoloside B at both medium (1.27 mM) and high (2.54 mM) doses had potent constipation prevention activities. Treatment with 3.25 mM hydroxytyrosol potently promoted gastrointestinal tract motility, whereas treatment with caffeic acid at 2.78 mM was in lower intestinal fluorescence intensity than that of the control group. The results also verified that not only the parent phenylethanoid glycosides, but also their *in vivo* degradation products, have the potential to be effective ingredients [21]. In addition, treatment of honokiol and magnolol at high dosage (3.67 μM) led to zebrafish intestinal fluorescence intensity at 89,647 and 87,452 pixels, respectively. Magnoflorine showed no activity at concentrations of 0.71, 1.43, and 2.86 μM. Although magnoflorine showed similar activity to magnolol in the molecular interaction analysis, the MTC values obtained by the assessment of honokiol in the zebrafish model might not be appropriate for magnoflorine. Thus, the ability of magnoflorine to prevent constipation in zebrafish models needs to be assessed in future studies. Molecular interaction analysis showed that magnolosides A, B, and D showed high affinities for the dopamine D2 receptor compared to domperidone, which was consistent with the results in the zebrafish model with domperidone as a positive drug. However, caffeic acid and hydroxytyrosol showed low affinities to the dopamine D2 receptor, however, potent activities in the zebrafish constipation model compared to domperidone, indicating that caffeic acid and hydroxytyrosol might target other targets to prevent constipation. For example, caffeic acid and hydroxytyrosol showed moderate affinities for the 5-HT_4 receptor in the current study.

4. Conclusion

TDAS, a tailored database-enhanced targeted screening strategy based on LC-HRMS fingerprints, was established to rapidly profile the *in vivo* metabolites of MOC and discover potent metabolites. Of these, 134 metabolites were characterized with high confidence levels. Moreover, 17 potential hit metabolites were rapidly discovered using molecular docking and molecular dynamic simulations. Among these, three were oxidized metabolites of prototypes, two were reduced metabolites of degradation products, five were isomerized metabolites of prototypes, and the others were prototypes or MOC parent compounds. The importance of this strategy was confirmed by *in vivo* bioactivity verification in a zebrafish constipation model, and seven metabolites were shown to have potent gastrointestinal tract motility. The TDAS approach can be applied to other TCMs for the rapid and efficient discovery of potent *in vivo* metabolites.

CRediT authorship contribution statement

Zhenzhen Xue: Writing – original draft, Validation, Software, Methodology, Investigation, Formal analysis, Data curation, Conceptualization. **Yudong Shang:** Validation, Investigation, Data curation. **Lan Yang:** Validation, Software. **Tao Li:** Validation, Investigation. **Bin Yang:** Writing – review & editing, Validation, Supervision, Conceptualization.

Declaration of competing interest

The authors declare that there are no conflicts of interest.

Acknowledgments

The work was supported by the Scientific and Technological Innovation Project of China Academy of Chinese Medical Sciences, China (Grant Nos.: CI2023E002 and CI2021A04513), the National Natural Science Foundation of China (Grant Nos.: 82204619 and 82274094), and the Fundamental Research Funds for the Central Public Welfare Research Institutes, China (Grant Nos.: ZZ15-YQ-067 and ZZ16-ND-10-26).

Appendix A. Supplementary data

Supplementary data to this article can be found online at https://doi.org/10.1016/j.jpha.2024.101066.

References

[1] X. Qiao, Y. Zhang, D. Guo, et al., Research methods and progress of effective components in traditional Chinese medicines, Sci. Sin. Vitae 52 (2022) 908–919.

[2] J.M. Matey, F. Zapata, L.M. Menéndez-Quintanal, et al., Identification of new psychoactive substances and their metabolites using non-targeted detection with high-resolution mass spectrometry through diagnosing fragment ions/neutral loss analysis, Talanta 265 (2023), 124816.
[3] Z. Xue, X. Zhang, H. Peng, et al., Exploration of habitat-related chemomarkers for Magnoliae Officinalis Cortex applying both global and water-soluble components-based metabolomics method, Phytomedicine 98 (2022), 153957.
[4] W.-L. Wei, H.-J. Li, W.-Z. Yang, et al., An integrated strategy for comprehensive characterization of metabolites and metabolic profiles of bufadienolides from Venenum Bufonis in rats, J. Pharm. Anal. 12 (2022) 136–144.
[5] W. Liu, W. Li, P. Zhang, et al., Quality structural annotation for the metabolites of chlorogenic acid in rat, Food Chem. 379 (2022), 132134.
[6] Q. Song, J. Li, H. Huo, et al., Retention time and optimal collision energy advance structural annotation relied on LC-MS/MS: An application in metabolite identification of an antidementia agent namely echinacoside, Anal. Chem. 91 (2019) 15040–15048.
[7] G. Feng, Z. Liu, S. Liu, et al., A target integration strategy for analyzing multidimensional chemical and metabolic substance groups of Ding-Zhi-Xiao-Wan prescription by using ultra-high performance liquid chromatography tandem mass spectrometry, J. Chromatogr. A 1608 (2019), 460412.
[8] F. Zhang, Z. Xie, X. Tang, et al., A combination of representative compounds, metabolism platform and diagnostic extraction strategy for characterization of metabolites of Shuang-Huang-Lian oral liquid *in vivo* by ultra-performance liquid chromatography coupled with time-of-flight mass spectrometry, J. Pharm. Biomed. Anal. 155 (2018) 216–234.
[9] C. Yu, F. Wang, X. Liu, et al., Corydalis Rhizoma as a model for herb-derived trace metabolites exploration: A cross-mapping strategy involving multiple doses and samples, J. Pharm. Anal. 11 (2021) 308–319.
[10] Y. Djoumbou-Feunang, J. Fiamoncini, A. Gil-de-la-Fuente, et al., BioTransformer: A comprehensive computational tool for small molecule metabolism prediction and metabolite identification, J. Cheminform. 11 (2019), 2.
[11] J. Zeng, Y. Li, C. Wang, et al., Combination of in silico prediction and convolutional neural network framework for targeted screening of metabolites from LC-HRMS fingerprints: A case study of "*Pericarpium Citri Reticulatae - Fructus Aurantii*", Talanta 269 (2024), 125514.
[12] Z. Xue, R. Yan, B. Yang, Phenylethanoid glycosides and phenolic glycosides from stem bark of *Magnolia officinalis*, Phytochemistry 127 (2016) 50–62.
[13] H. Luo, H. Wu, X. Yu, et al., A review of the phytochemistry and pharmacological activities of Magnoliae Officinalis Cortex, J. Ethnopharmacol. 236 (2019) 412–442.
[14] C. Xie, W. Hu, L. Gan, et al., Sulfation and its effect on the bioactivity of magnolol, the main active ingredient of *Magnolia officinalis*, Metabolites 12 (2022), 870.
[15] Y. Dong, M. Tang, H. Song, et al., Characterization of metabolic profile of honokiol in rat feces using liquid chromatography coupled with quadrupole time-of-flight tandem mass spectrometry and ^{13}C stable isotope labeling, J. Chromatogr. B Analyt. Technol. Biomed. Life Sci. 953–954 (2014) 20–29.
[16] Z. Xue, C. Wu, J. Wei, et al., An orally administered magnoloside A ameliorates functional dyspepsia by modulating brain-gut peptides and gut microbiota, Life Sci. 233 (2019), 116749.
[17] Z. Xue, C. Lai, L. Kang, et al., Profiling and isomer recognition of phenylethanoid glycosides from *Magnolia officinalis* based on diagnostic/holistic fragment ions analysis coupled with chemometrics, J. Chromatogr. A 1611 (2020), 460583.
[18] J. Zhang, H. Li, L. Hou, et al., Pharmacokinetics and metabolites of glycosides and lignans of the stem bark of *Magnolia officinalis* in functional dyspepsia and normal rats using liquid chromatography-tandem mass spectrometry, J. Sep. Sci. 45 (2022) 3663–3678.
[19] D. Bui, L. Li, T. Yin, et al., Pharmacokinetic and metabolic profiling of key active components of dietary supplement *Magnolia officinalis* extract for prevention against oral carcinoma, J. Agric. Food Chem. 68 (2020) 6576–6587.
[20] T. Nakazawa, T. Yasuda, K. Ohsawa, Metabolites of orally administered *Magnolia officinalis* extract in rats and man and its antidepressant-like effects in mice, J. Pharm. Pharmacol. 55 (2003) 1583–1591.
[21] Z. Xue, B. Yang, Phenylethanoid glycosides: Research advances in their phytochemistry, pharmacological activity and pharmacokinetics, Molecules 21 (2016), 991.
[22] J. Guo, T. Huan, Comparison of full-scan, data-dependent, and data-independent acquisition modes in liquid chromatography-mass spectrometry based untargeted metabolomics, Anal. Chem. 92 (2020) 8072–8080.
[23] G.M. Morris, R. Huey, W. Lindstrom, et al., AutoDock4 and AutoDockTools4: Automated docking with selective receptor flexibility, J. Comput. Chem. 30 (2009) 2785–2791.
[24] M.F. Adasme, K.L. Linnemann, S.N. Bolz, et al., PLIP 2021: Expanding the scope of the protein-ligand interaction profiler to DNA and RNA, Nucleic Acids Res. 49 (2021) W530–W534.
[25] The Amber Home Page, Amber 2020 Reference Manual (Covers Amber20 and AmberTools20), https://ambermd.org/doc12/Amber20.pdf. (Accessed 24 May 2024).
[26] Z. Xue, L. Xu, Z. Shang, et al., Discovery of minor quality evaluation marker compounds for Chinese patent medicine products using a two-leveled metabolomics strategy, J. Chromatogr. A 1652 (2021), 462354.
[27] M. Hattori, T. Sakamoto, Y. Endo, et al., Metabolism of magnolol from Magnoliae Cortex. I. Application of liquid chromatography-mass spectrometry to the analysis of metabolites of magnolol in rats, Chem. Pharm. Bull. (Tokyo) 32 (1984) 5010–5017.
[28] Z. Xue, H. Li, B. Yang, Positional isomerization of phenylethanoid glycosides from *Magnolia officinalis*, Nat. Prod. Commun. 11 (2016) 1861–1863.
[29] Y. Wang, H. Hao, G. Wang, et al., An approach to identifying sequential metabolites of a typical phenylethanoid glycoside, echinacoside, based on liquid chromatography-ion trap-time of flight mass spectrometry analysis, Talanta 80 (2009) 572–580.
[30] Y. Li, G. Zhou, S. Xing, et al., Identification of echinacoside metabolites produced by human intestinal bacteria using ultraperformance liquid chromatography-quadrupole time-of-flight mass spectrometry, J. Agric. Food Chem. 63 (2015) 6764–6771.
[31] N. Ye, M. Tang, H. Ye, et al., ^{13}C stable isotope labeling followed by ultra-high performance liquid chromatography/quadrupole time-of-flight tandem mass spectrometry (UHPLC/Q-TOF MS) was applied to identify the metabolites of honokiol in rat small intestines, Anal. Methods 7 (2015) 2488–2496.
[32] X. Tian, Y. Zhang, Z. Li, et al., Systematic and comprehensive strategy for metabolite profiling in bioanalysis using software-assisted HPLC-Q-TOF: Magnoflorine as an example, Anal. Bioanal. Chem. 408 (2016) 2239–2254.
[33] C. You, Y. Zhang, Y. Xu, et al., Structural basis for motilin and erythromycin recognition by motilin receptor, Sci. Adv. 9 (2023), eade9020.
[34] S. Huang, P. Xu, D.-D. Shen, et al., GPCRs steer G_i and G_s selectivity via TM5-TM6 switches as revealed by structures of serotonin receptors, Mol. Cell 82 (2022) 2681–2695.e6.
[35] D. Im, A. Inoue, T. Fujiwara, et al., Structure of the dopamine D2 receptor in complex with the antipsychotic drug spiperone, Nat. Commun. 11 (2020), 6442.
[36] Y. He, S. Zhu, C. Wu, et al., Bioactivity-guided separation of potential D_2 dopamine receptor antagonists from Aurantii Fructus based on molecular docking combined with high-speed counter-current chromatography, Molecules 23 (2018), 3135.
[37] L.E. Kuil, R.K. Chauhan, W.W. Cheng, et al., Zebrafish: A model organism for studying enteric nervous system development and disease, Front. Cell Dev. Biol. 8 (2021), 629073.
[38] A. Rich, A new high-content model system for studies of gastrointestinal transit: The zebrafish, Neurogastroenterol. Motil. 21 (2009) 225–228.
[39] Y. Lu, Z. Zhang, X. Liang, et al., Study of gastrointestinal tract viability and motility via modulation of serotonin in a zebrafish model by probiotics, Food Funct. 10 (2019) 7416–7425.